Engineering Structures 140 (2017) 98–109

Contents lists available at ScienceDirect

Engineering Structures

journal homepage: www.elsevier.com/locate/engstruct

New nonlinear lateral-vertical coupled shear element model for use in finite element structural analysis applications

Thang N. Dao [a,*], John W. van de Lindt [b], Tu X. Ho [a]

[a] Department of Civil, Construction and Environmental Engineering, The University of Alabama, AL, USA
[b] George T. Abell Professor in Infrastructure, Department of Civil and Environmental Engineering, Colorado State University, Fort Collins, CO, USA

ARTICLE INFO

Article history:
Received 1 September 2016
Revised 24 February 2017
Accepted 26 February 2017
Available online 9 March 2017

Keywords:
Shear element
Light-frame structures
P-Δ effect
Geometric nonlinearity
Nonlinear static analysis
Earthquake engineering

ABSTRACT

In nonlinear structural analysis, shear walls within whole-system models are often modeled using a spring model with a single degree of freedom where the lateral stiffness of the shear wall is modeled as a nonlinear spring. The stiffness of the spring is often described by the hysteretic relationship between the lateral restoring force and shear wall lateral deformation. In this study, a new shear element is introduced, which couples the lateral and vertical stiffness of the shear wall. This new shear element is able to better describe the behavior of shear walls in mid-rise and tall buildings. An illustrative example is presented to help explain the application of the new shear element in finite element modeling. In the examples, the new shear element is used to calculate displacement and internal forces for cold-formed steel frames. The results show that without including vertical wall stiffness, the lateral displacement is significantly underestimated. The difference increases with the height of the building and for a ten-story frame the new model demonstrates an increased lateral displacement at roof level of 64.1% when compared with current typical shear element model (lateral stiffness only).

1. Introduction

Shear wall systems play an important role in buildings subjected to lateral loading since their high capacity allows them to resist lateral load while still carrying gravity load. Over the past few decades, many studies have focused on shear wall modeling for light-frame structures, including wood and cold-form steel light-frame buildings. A detailed model was developed by Collins et al. [1], in which a pair of diagonal hysteretic nonlinear springs was used to describe in-plane behavior of a light-frame shear wall. Plate element and beam elements were used to represent the sheathing and frame, respectively. The frame intersections were modeled as pinned connections. Thus, the model can take account of the out-of-plane action of shear walls. Folz and Filiatrault [2] did an analysis of a wood shear wall under cyclic loading. In that study, the sheathing-to-framing connector behavior was modeled by a ten-parameter hysteretic model. This hysteretic model included pinching behavior and strength and stiffness degradation due to cyclic loading, resulting in the model capturing the behavior of wood shear walls very well. The result from the cyclic loading analysis can be used to model wood shear walls as a single degree of freedom spring, which can then be utilized in a 3-D model of a building for non-linear time history analysis of light-frame wood buildings. Based on the Folz and Filiatrault [2] hysteretic model, Pang et al. [3] developed an evolutionary parameter hysteretic model (EPHM) using sixteen parameters for modeling wood frame structures. This new hysteretic model included the degradation of the backbone curve itself as well as degradation of the unloading stiffness. Pei and van de Lindt [4] applied this EPHM in their study to develop a coupled shear-bending formulation for seismic analysis of multi-story wood shear wall systems. In that study, the shear walls were modeled using 3-D uncoupled springs and the stiffness of the shear wall and tie-down system in a story was lumped into representative story stiffness. A 3D building model was developed in ABAQUS by Xu and Dolan [5]. In this study, the single hysteretic spring model, which was similar to Folz and Filiatrault's model [2], was used to estimate spring parameter. Then, the diagonal-spring shear wall model, which was used in Collins's study [1], was applied for final simulation.

In addition to wood shear-wall modeling, there have been studies focusing on modeling of cold-formed steel shear walls. Kim et al. [6] conducted a shake table test of a two-story, one-bay structure with X-straps attached to resist the lateral load. The response measured during the test was then compared with numerically calculated values. In the numerical study, the columns were modeled using beam elements and the non-linear behavior was

* Corresponding author at: Department of Civil, Construction, and Environmental Engineering, University of Alabama, Tuscaloosa, AL 35487-0205, USA.
E-mail address: tndao@eng.ua.edu (T.N. Dao).

http://dx.doi.org/10.1016/j.engstruct.2017.02.064
0141-0296/

modeled using an inelastic rotational spring. The X-straps were modeled using inelastic truss elements with gap properties, which were assigned a bilinear hysteretic stiffness. In another study, Pastor and Rodríguez-Ferran [7] modeled X-braced shear walls by treating panels as single-degree-of-freedom (SDOF) structures. In their numerical model, only lateral force and lateral displacement were considered and the structure was also modeled using a bilinear hysteretic oscillator. They conducted non-linear time history analysis to compare the results between SDOF and multi-degrees-of-freedom (MODF) models. The results showed a good agreement for one-story X-braced shear walls between the two cases. Moreover, in a study in wall-stud cold-formed shear panels sheeted with corrugated sheeting and OSB, Fulop and Dubina [8] proposed a single degree of freedom system (SDOF) with a fiber-hinge accommodating the desired hysteretic behavior. The wall-stud cold-formed shear panel can be replaced with a pinned rectangular frame with dissipative diagonals. The hysteretic behavior was described by a tri-linear or a nonlinear model. The SDOF model was accurate enough to describe all the important aspects of the hysteretic behavior and simple enough to be integrated into global structural modeling. Similarly, other studies [9,10] modeled the shear wall, including steel sheathing and screw connections, by truss elements using the Pinching 04 material property in OpenSees software. The shear wall was modeled as a pin-connected panel with two diagonals. The model was validated and calibrated using a series of full-scale shake table tests for five single-story walls and five double-story walls (Shamim and Rogers, [9]). After that, the model was tested for a 3D 2-story building under displacement-controlled pushover analysis, nonlinear time history analysis, and IDA (Leng et al. [10]). Another approach was introduced by Martínez-Martínez and Xu [11], who developed a flat shell element with equivalent properties to model complete shear panels. The shell element was considered as a 16-node natural orthotropic element, and then the stiffness matrices for both linear and nonlinear analysis were derived.

Even though there have been numerous studies related to shear wall modeling for light-frame structures, most of these studies model shear walls using a spring model that considers lateral displacement as a SDOF. While the results from these studies help to reduce the number of degrees of freedom (DOF) for nonlinear time history analysis, and the modeling philosophy works well for shorter (e.g., one to four stories) buildings, it does not accurately model the vertical displacement on each side of the shear wall element in taller buildings. In mid-rise and tall buildings, the local and global overturning moments often cause additional vertical displacement of the hold-down rods in stacked wood shear walls or columns in a cold-formed steel frame system. This additional vertical displacement, in turn, causes larger lateral displacements and P-Δ effects.

In this study, a new shear element for light-frame structures is introduced to couple the lateral and vertical stiffness. With this coupled shear spring element, the effect of lateral displacement on the vertical component and the effect of the vertical component on lateral displacement are included. Non-linear behavior of the shear wall can be described by the lateral stiffness which is also included in the shear element stiffness matrix and the effect of large displacements will be discussed in detail later. The new model will allow predicting more accurate lateral displacement using experiment data. The effect of non-structural components can be included in the model if the test specimen includes non-structural components.

Moreover, the proposed shear element helps to reduce time and simplify the procedure in modeling. In finite element modeling, many researchers have tried to model substructures using super elements. Petersson and Popov [12] introduced a procedure called matrix condensation to systematically reduce the number of assembled equations on different substructure levels. Lee et al. [13] proposed a method using this substructuring technique and matrix condensation to analyze high-rise box system structures considering the effects of floor slabs. Kim and Lee [14] used the condensation technique to model concrete shear walls with openings. The condensation technique is well-known in structural dynamics and is essentially a technique that helps to reduce the number of nodes in a typical structural component model by pre-solving some of the equations of equilibrium for that typical component. This technique is helpful in a structure that has linear behavior under dynamic loading. For nonlinear structural dynamics, the stiffness matrix of the structure varies with time (or displacement), and therefore the condensation would need to be conducted at every time step after the stiffness matrix of the component has been estimated. Obviously under such a scenario the condensation technique would not help to reduce computational cost. The stiffness of the shear element introduced in this study is evaluated through the lateral stiffness and the dimension of the shear wall. Therefore, the substructuring and matrix condensation techniques are unnecessary. While no condensation technique is needed, the hysteretic parameters of the lateral stiffness of the shear wall must be provided.

2. Derivation of shear element stiffness matrix

In past studies, the lateral stiffness and non-linear behavior of a shear wall are often evaluated through its hysteresis. This hysteresis is often obtained either by numerical model starting at the nonlinear model for nails [2] or by reversed cyclic tests of a shear wall [3,5,7,9]. In both these types of studies, numerical or experimental, the vertical displacement was assumed to be zero. In the current study, a stiffness matrix of a new shear element coupling both lateral and vertical stiffness is introduced. To do this, it is first assumed that there is only lateral displacement of the 4-node shear element, and the force acting on each side of the shear element is calculated. Then, the effect of vertical displacement on the lateral force is derived. The force on each side of the shear element is then transferred into the nodes as a function of lateral and vertical displacement of the shear element. The shear element stiffness matrix is evaluated based on the relationship between the nodal force and nodal displacement just derived.

Consider Fig. 1 showing the interactive forces acting on a 4-node shear element in the x and y direction. Let the total shear force acting in the x direction be F_x and in the y direction be F_y. Then,

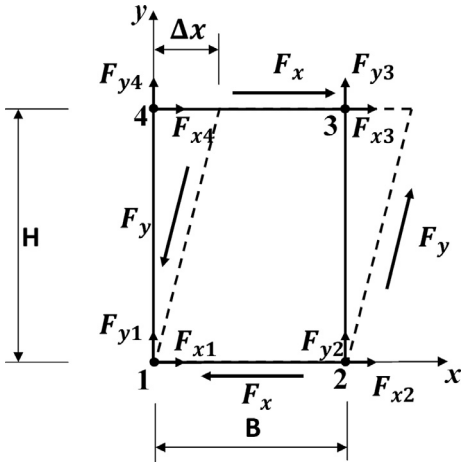

Fig. 1. Interactive forces acting on shear element.

$$F_x = -(F_{x1} + F_{x2}) = F_{x3} + F_{x4} \tag{1a}$$

$$F_y = -(F_{y1} + F_{y4}) = F_{y2} + F_{y3} \tag{1b}$$

Now assume that the shear element deforms only in the x direction and there is no vertical displacement, or $\Delta x \neq 0$ and $\Delta y = 0$. By the equilibrium condition of the moment about the z axis, $\Sigma M_z = 0$, one simply has

$$F_y = \frac{H}{B} F_x = \frac{H}{B} k_{xx} \Delta x \tag{2}$$

where k_{xx} is the stiffness of the shear element in the x direction due to displacement Δx; B and H are dimensions of the panel in x and y direction, respectively. Eq. (2) is then used to determine the vertical force transferred to the columns due to lateral displacement Δx.

Similarly, in the case that $\Delta x = 0$ and $\Delta y \neq 0$, one can have:

$$F_x = \frac{B}{H} k_{yy} \Delta y \tag{3}$$

$$F_y = k_{yy} \Delta y \tag{4}$$

Combining (2), (3) and (4) and rewriting in matrix form, gives

$$\begin{Bmatrix} F_x \\ F_y \end{Bmatrix} = \begin{bmatrix} k_{xx} & \frac{B}{H} k_{yy} \\ \frac{H}{B} k_{xx} & k_{yy} \end{bmatrix} \begin{Bmatrix} \Delta x \\ \Delta y \end{Bmatrix} \tag{5}$$

From the principle of the virtual work, the stiffness matrix is symmetrical about the main diagonal, that gives:

$$\begin{aligned} &\tfrac{B}{H} k_{yy} = \tfrac{H}{B} k_{xx} \\ &\text{or} \quad k_{yy} = \tfrac{H^2}{B^2} k_{xx} \end{aligned} \tag{6}$$

Rewriting Eq. (5) gives

$$\begin{aligned} &\begin{Bmatrix} F_x \\ F_y \end{Bmatrix} = k_{xx} \begin{bmatrix} 1 & \frac{H}{B} \\ \frac{H}{B} & \frac{H^2}{B^2} \end{bmatrix} \begin{Bmatrix} \Delta x \\ \Delta y \end{Bmatrix} \\ &\text{or} \quad [F_s] = [K_s]\{U_s\} \end{aligned} \tag{7}$$

where

$$\{F_s\} = \begin{Bmatrix} F_x \\ F_y \end{Bmatrix}; [K_s] = k_{xx} \begin{bmatrix} 1 & \frac{H}{B} \\ \frac{H}{B} & \frac{H^2}{B^2} \end{bmatrix}; \text{and} \{U_s\} = \begin{Bmatrix} \Delta x \\ \Delta y \end{Bmatrix} \tag{8}$$

Transferring the shear-force and shear displacement acting on each side of the shear element to the nodes, gives

$$\begin{aligned} &\{F_e\} = [A]\{F_s\} \\ &\{U_e\} = [A]\{U_s\} \end{aligned} \tag{9}$$

where $\{F_e\}$ is the element force vector; $\{U_e\} = [u_1 \quad v_1 \quad u_2 \quad v_2 \quad u_3 \quad v_3 \quad u_4 \quad v_4]^T$ is the element displacement vector; and $[A]$ is the nodal weighted matrix,

$$[A] = \begin{bmatrix} w_{x1} & 0 & w_{x2} & 0 & w_{x3} & 0 & w_{x4} & 0 \\ 0 & w_{y1} & 0 & w_{y2} & 0 & w_{y3} & 0 & w_{y4} \end{bmatrix}^T \tag{10}$$

where w_{x1}, w_{x2}, w_{x3}, w_{x4}, w_{y1}, w_{y2}, w_{y3} and w_{y4} are the nodal weighted values of shear element nodes 1, 2, 3 and 4 in the x and y directions, respectively. These values are functions of the nodal stiffness distribution within the shear element and: $w_{x1} + w_{x2} = -1$; $w_{x3} + w_{x4} = 1$; $w_{y1} + w_{y4} = -1$; and $w_{y2} + w_{y3} = 1$. For a structural element which has symmetric stiffness in both the x and y direction: $w_{x1} = w_{x2} = w_{x3} = w_{x4} = 0.5$; $w_{y1} = w_{y4} = w_{y2} = w_{y3} = 0.5$. While nodal weighted values affect the local axial force in columns, these values do not affect the total axial force F_y that the shear element transfers to the next story level of the columns. Finally, substituting Eq. (9) into Eq. (7), gives

$$\begin{aligned} &\{F_e\} = [A][K_s][A]^T\{X_e\} \\ &\{F_e\} = [K_e]\{X_e\} \\ &[K_e] = [A][K_s][A]^T \end{aligned} \tag{11}$$

where $[K_e]$ is the nodal shear element stiffness matrix. For a linear shear element, the stiffness k_{xx} is taken as a constant value.

2.1. Non-linear behavior modeling consideration

The non-linear behavior of a shear wall can be described through the lateral stiffness k_{xx} in Eqs. (2)-(8). This stiffness is often obtained by the force and displacement relationship presented by the hysteresis resulting from either the numerical model or testing program. During the test, the lateral stiffness is a function of lateral displacement while the vertical displacement is assumed to be zero. In the shear element, the change in lateral stiffness k_{xx} should include the effect of vertical displacement. Fig. 2 shows the geometric relationship between the equivalent lateral displacement of the wall during the test (no vertical displacement) and the displacements Δx and Δy of the shear element. It is assumed that the displacements are small enough such that:

$$\begin{aligned} &\alpha + \beta \approx \tan(\alpha + \beta) \approx \tan(\alpha) + \tan(\beta) \\ &\text{or :} \quad \tfrac{x_{eq}}{H} = \tfrac{\Delta x}{H} + \tfrac{\Delta y}{B} \end{aligned} \tag{12}$$

where x_{eq} is the equivalent lateral displacement that is used to evaluate the stiffness k_{xx} from the hysteresis describing the relationship between lateral displacement and lateral force of the shear wall typically obtained from experiment. Eq. (12) gives:

$$x_{eq} = \Delta x + \frac{H}{B} \Delta y \tag{13}$$

From the equivalent lateral displacement x_{eq}, one can evaluate the stiffness k_{xx} by using the hysteretic relationship as mentioned above. In non-linear time history analysis, the stiffness k_{xx} is often evaluated as the tangential stiffness, or:

$$k_{xx} = \frac{\Delta F_{hys}}{\Delta x_{eq}} \tag{14}$$

where ΔF_{hys} and Δx_{eq} are the change in hysteretic force and equivalent lateral displacement at a specific time step, respectively.

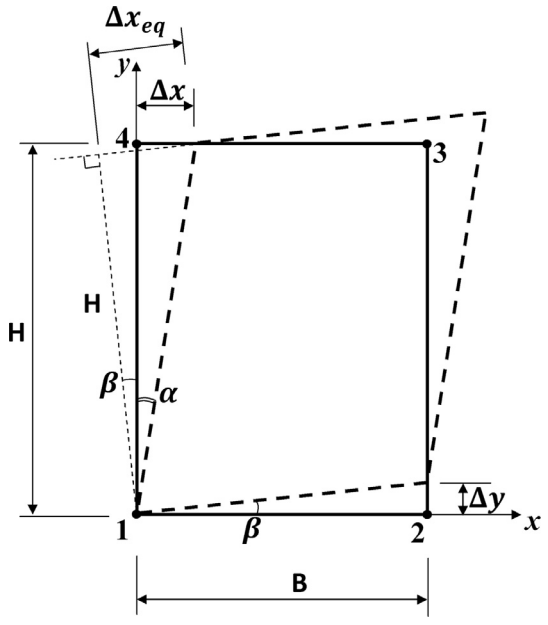

Fig. 2. Equivalent lateral displacement.

2.2. Effect of large deformation

In the previous section, the shear element stiffness matrix is derived with the assumption that the nodal forces in the shear element are applied at the original nodal coordinates. In reality, when the structure deforms, the position of the forces acting on each node also moves with the structure and the equilibrium condition is different from that of the original position. This is especially true for large deformations, the distance between nodes within the shear element changes significantly causing considerable variation in the nodal forces. During an earthquake, structures can experience large lateral displacements. For this reason, additional force acting on each node of the shear element due to the effects of large deformation should be included. This section presents the derivation of the geometric stiffness matrix for the shear element to account for large displacement in both lateral and vertical directions.

Now, consider that when a structure deforms under a certain load case, a shear wall has displacement Δx and Δy in the x and y direction, respectively. One can see that in Fig. 3, the nodal forces are shown on the deformed element while in Fig. 1 these forces are shown on the original shape of the shear element. Because of that, the P-Δ effect must be taken into account. This effect causes additional moments to the shear wall, that can be represented by additional shear forces. The large displacement in the x direction causes additional lateral shear forces (in the x direction) while the large displacement in the y direction induces the additional vertical shear force (in the y direction). Fig. 3 shows the additional shear forces acting on each side of the shear element due to large displacements in the x and y directions, respectively.

Consider that the shear element deforms only in the x direction and there is no vertical displacement, or $\Delta x \neq 0$ and $\Delta y = 0$. The additional moment about z-axis at node 1 due to the P-Δ effect:

$$M_z^{\Delta} = (F_{y3} + F_{y4})\Delta x \tag{15a}$$

This moment will be balanced by an additional shear force:

$$F_x^{\Delta} = F_{43}^{\Delta} = \frac{M_z^{\Delta}}{H} = \frac{(F_{y3} + F_{y4})}{H}\Delta x \tag{15b}$$

If the moment equilibrium equation is written about z-axis at node 4:

$$F_x^{\Delta} = F_{12}^{\Delta} = \frac{M_z^{\Delta}}{H} = \frac{(F_{y1} + F_{y2})}{H}\Delta x \tag{15c}$$

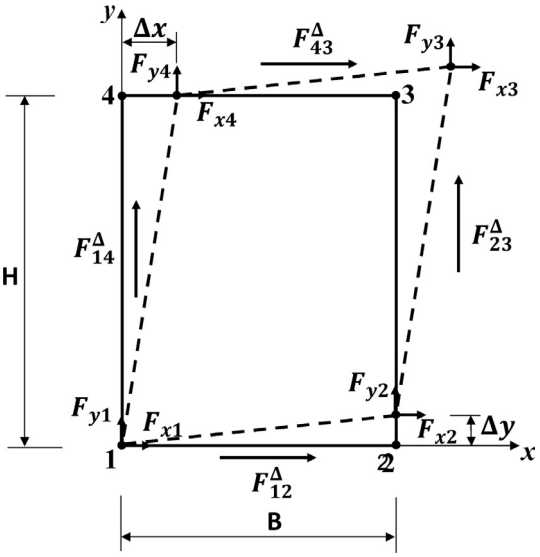

Fig. 3. Interactive forces acting on shear element for large displacement effect.

There is no additional shear force created in y-direction:

$$F_{23}^{\Delta} = F_{14}^{\Delta} = 0 \tag{15d}$$

Similarly, if the shear element deforms only in the y direction, and there is no lateral displacement ($\Delta y \neq 0$ and $\Delta x = 0$), the following equations can be obtained:

$$F_{23}^{\Delta} = \frac{(F_{x2} + F_{x3})}{B}\Delta y \tag{16a}$$

$$F_{14}^{\Delta} = \frac{(F_{x1} + F_{x4})}{B}\Delta y \tag{16b}$$

$$F_{12}^{\Delta} = F_{43}^{\Delta} = 0 \tag{16c}$$

Combining the effects in x- and y- directions:

$$\begin{aligned} F_{12}^{\Delta} &= \tfrac{F_{y1}+F_{y2}}{H}\Delta x \\ F_{23}^{\Delta} &= \tfrac{F_{x2}+F_{x3}}{B}\Delta y \\ F_{43}^{\Delta} &= \tfrac{F_{y3}+F_{y4}}{H}\Delta x \\ F_{14}^{\Delta} &= \tfrac{F_{x1}+F_{x4}}{B}\Delta y \end{aligned} \tag{17}$$

Recall that from the equilibrium condition of the nodal forces in x and y direction, one can have:

$$\begin{aligned} \textstyle\sum_i F_{xi} &= F_{x1} + F_{x2} + F_{x3} + F_{x4} = 0 \text{ or } F_{x1} + F_{x4} = -(F_{x2} + F_{x3}) \\ \textstyle\sum_i F_{yi} &= F_{y1} + F_{y2} + F_{y3} + F_{y4} = 0 \text{ or } F_{y1} + F_{y2} = -(F_{y3} + F_{y4}) \end{aligned} \tag{18}$$

Letting:

$$\begin{aligned} K_x^{\Delta} &= \tfrac{F_{y3}+F_{y4}}{H} \\ K_y^{\Delta} &= \tfrac{F_{x2}+F_{x3}}{B} \end{aligned} \tag{19}$$

In which: K_x^{Δ} and K_y^{Δ} are geometric stiffness components of the shear element in x- and y- directions, respectively.

Rewriting Eq. (17) in matrix form with consideration of Eqs. (18) and (19), gives:

$$\begin{Bmatrix} F_{12}^{\Delta} \\ F_{23}^{\Delta} \\ F_{43}^{\Delta} \\ F_{14}^{\Delta} \end{Bmatrix} = \begin{bmatrix} -1 & 0 \\ 0 & 1 \\ 1 & 0 \\ 0 & -1 \end{bmatrix} \begin{bmatrix} K_x^{\Delta} & 0 \\ 0 & K_y^{\Delta} \end{bmatrix} \begin{Bmatrix} \Delta x \\ \Delta y \end{Bmatrix} = [C]\left[K_s^{\Delta}\right]\{U_s\} \tag{20}$$

where $[C] = \begin{bmatrix} -1 & 0 \\ 0 & 1 \\ 1 & 0 \\ 0 & -1 \end{bmatrix}$ and $\left[K_s^{\Delta}\right] = \begin{bmatrix} K_x^{\Delta} & 0 \\ 0 & K_y^{\Delta} \end{bmatrix}$. Transferring these forces to the nodes of the shear element gives:

$$\begin{Bmatrix} F_{x1}^{\Delta} \\ F_{y1}^{\Delta} \\ F_{x2}^{\Delta} \\ F_{y2}^{\Delta} \\ F_{x3}^{\Delta} \\ F_{y3}^{\Delta} \\ F_{x4}^{\Delta} \\ F_{y4}^{\Delta} \end{Bmatrix} = \begin{bmatrix} w_{x1} & 0 & 0 & 0 \\ 0 & 0 & 0 & w_{y1} \\ w_{x2} & 0 & 0 & 0 \\ 0 & w_{y2} & 0 & 0 \\ 0 & 0 & w_{x3} & 0 \\ 0 & w_{y3} & 0 & 0 \\ 0 & 0 & w_{x4} & 0 \\ 0 & 0 & 0 & w_{y4} \end{bmatrix} \begin{Bmatrix} F_{12}^{\Delta} \\ F_{23}^{\Delta} \\ F_{43}^{\Delta} \\ F_{14}^{\Delta} \end{Bmatrix} \tag{21}$$

Then the combination of Eqs. (9), (20) and (21) gives:

$$\left\{F_e^{\Delta}\right\} = [D][C]\left[K_s^{\Delta}\right][A]^T\{U_e\} \tag{22}$$

where

$$[D] = \begin{bmatrix} w_{x1} & 0 & 0 & 0 \\ 0 & 0 & 0 & w_{y1} \\ w_{x2} & 0 & 0 & 0 \\ 0 & w_{y2} & 0 & 0 \\ 0 & 0 & w_{x3} & 0 \\ 0 & w_{y3} & 0 & 0 \\ 0 & 0 & w_{x4} & 0 \\ 0 & 0 & 0 & w_{y4} \end{bmatrix}.$$

Because $[D][C] = [A]$, Eq. (22) can be rewritten as:

$$\begin{aligned} \left\{F_e^{\Delta}\right\} &= [A]\left[K_s^{\Delta}\right][A]^T\{U_e\} = \left[K_e^{\Delta}\right]\{U_e\} \\ \left[K_e^{\Delta}\right] &= [A]\left[K_s^{\Delta}\right][A]^T \end{aligned} \tag{23}$$

where $\left[K_e^{\Delta}\right]$ is the geometric stiffness matrix of the shear element.

3. Additional considerations

As one can see from the previous section, the geometric stiffness matrix of the shear element depends on its nodal forces. In turn these nodal forces are calculated based on the element stiffness and nodal displacement. Therefore, the analysis process relates to the so-called geometric nonlinearity. From the derivation of elastic stiffness and geometric stiffness presented above, it can be seen that the effects of both geometric and material nonlinearity can be included. In some cases, the shear element has symmetric stiffness properties that induce identical nodal weight values, or $w_{x1} = w_{x2} = w_{x3} = w_{x4} = 0.5$; $w_{y1} = w_{y4} = w_{y2} = w_{y3} = 0.5$ which leads to $F_{x2} = -F_{x3}$ and $F_{y3} = -F_{y4}$; for this reason, from Eq. (19) one can see that the stiffness $K_x^{\Delta} = K_y^{\Delta} = 0$ or geometric stiffness of the shear wall element is equal to zero. In such a case, the large displacement of the shear element does not affect the equilibrium conditions, and the internal nodal forces depend only on the elastic stiffness. In general, the shear element geometric stiffness matrix only accounts for the effects of large displacement within the shear element and does not account for the global *P-Δ* effect.

It should be noted that the shear element introduced in this study is used to present the shear behavior of the shear wall only. Both the elastic and geometric stiffness matrices shown in Eqs. (11) and (23) do not include the stiffness (axial stiffness) along each side of the shear element. In some cases, a truss element can be used to model the axial stiffness between two nodes on each side of the shear element. For example, in cold-form steel modeling applications that will be discussed in a later illustrative example, the shear wall panels are attached to the columns and carry the floor loading. In such a case, the shear element can be used to model the shear wall panel and the column is modeled as a beam element and represents the stiffness between two nodes on each side of the shear element. On the side where the shear wall panel is attached to the floor, a solid truss element can be used to constrain the movement between the two nodes on each side because the floor stiffness is so high in the axial direction. In the application for wood shear wall modeling, while the shear behavior of the wall can be modeled using a shear element, the hold-down rod can be represented using a bi-linear truss element that has different stiffness when experiencing tension and compression, respectively. Specifically, in tension, the stiffness of this truss element is equal to the tension stiffness of the hold-down rod, and the compression stiffness of the truss element is equal to the compression stiffness of the wood studs that carry the compression load.

In the case where beam or truss element is used to model the axial stiffness of each side of the shear element, if the geometric stiffness of the beam or truss element is included, both local and global $P-\Delta$ effects will be picked up automatically, which will be examined in more detail later.

4. Example and discussion

4.1. A comparison based on a five story frame

In order to examine how the shear element works in a numerical model, a five-story cold-form steel frame was analyzed in this example. Fig. 4a shows the original model of the frame with a line drawing of truss and column members. In a traditional finite element model, one would model the cold-formed steel members and columns as truss or beam elements, and the connection between members would be assumed to behave as a hinged or fixed node. A more complex model may consider connections as nonlinear springs to describe the behavior of the connection under a certain load case. While such models can model the behavior of the frame resulting in good accuracy, they also can include a large number of DOFs and lead to time-consuming computation for nonlinear time history analysis of a full building model. If the conventional shear wall model is used, the shear wall panel with a V-brace (see Fig. 5a) would be modeled as a SDOF spring, which helps reduce the computational effort. But as mentioned, since it does not include the vertical displacement effect, the lateral displacement will not be estimated accurately and there is no vertical force due to lateral displacement transferred to the columns.

In this example, the cold-formed steel frame shown in Fig. 4a will be analyzed under different load cases with the application of the new shear element introduced in this study. The dimensions of the cross section of the columns used in this example are shown in Fig. 4a. The columns are modeled by the beam element and connected to shear elements by pinned connections. Thus, shear elements only work under shear behavior and transfer the loads in both lateral and vertical directions to columns. The analysis of the frame under vertical load (Fig. 4b), lateral load (Fig. 4c), combination of vertical and lateral loads, and displacement-controlled cyclic loads will be examined here. In the application of the new shear element, the stiffness k_{xx} in Eq. (2) needs to be determined prior to the numerical analysis using Eq. (14).

A single V-braced panel was tested under cyclic loading (Fig. 5b) to provide the experimental hysteresis for use in this paper as well as validate the super shear model. The V-braced panel was 2.44 m (8ft) long and 3.2 m (10.5ft) high. During the test, the panel was attached to two columns as it would be in an actual building. The columns were made of cold-formed steel with HSS square section 8.9 × 8.9 × 0.95 cm (3.5 × 3.5 × 0.375in). The V-braced panel was connected to the floor and columns at both sides by screw connections which provided the energy dissipation components to the total panel hysteresis. A load frame was designed specifically for this test (Fig. 5a) because two pinned supports was attached to the columns to remove the lateral capacity of the columns during the tests and isolate the V-braced panel behavior, since the behavior of the column itself is well understood and will be modeled using typical finite elements. The maximum vertical displacement on the top of the columns was insignificant (about 0.003in) during the test, therefore the hysteresis data can be used to estimate k_{xx} from Eq. (14). Interested readers can refer to Dao and Van de Lindt [15] for more details in the experiment.

The experimental data also helps to validate the Eq. (2). Fig. 6 shows the comparison of the force transferred to columns measured from the experiment of 4ft V-braced panel and the force calculated by Eq. (2) in which the lateral force F_x is equal to the load recorded from the actuator. It can be seen that at the beginning, the force calculated from Eq. (2) is greater than the force measured by

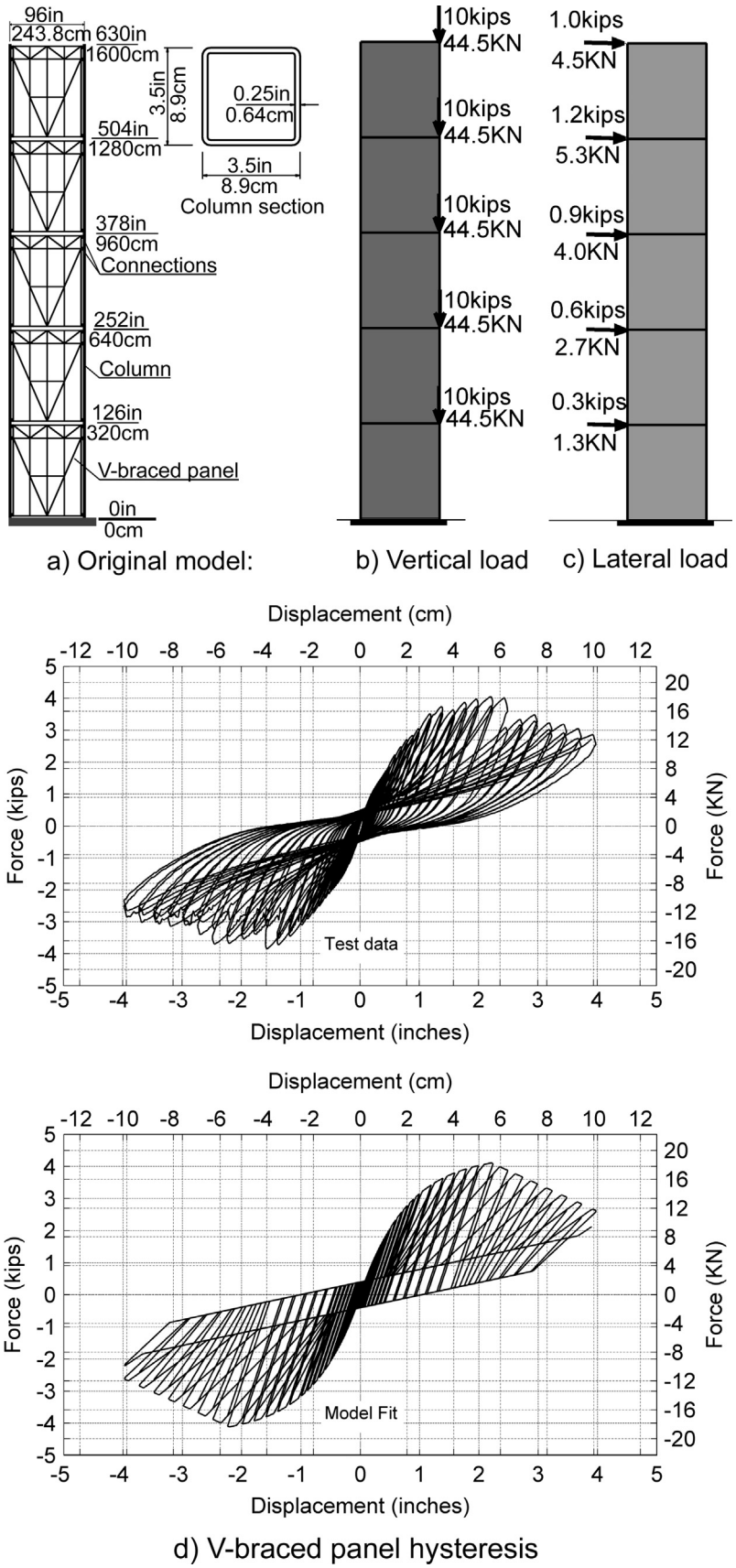

Fig. 4. Frame model, load cases and panel hysteresis used in the example.

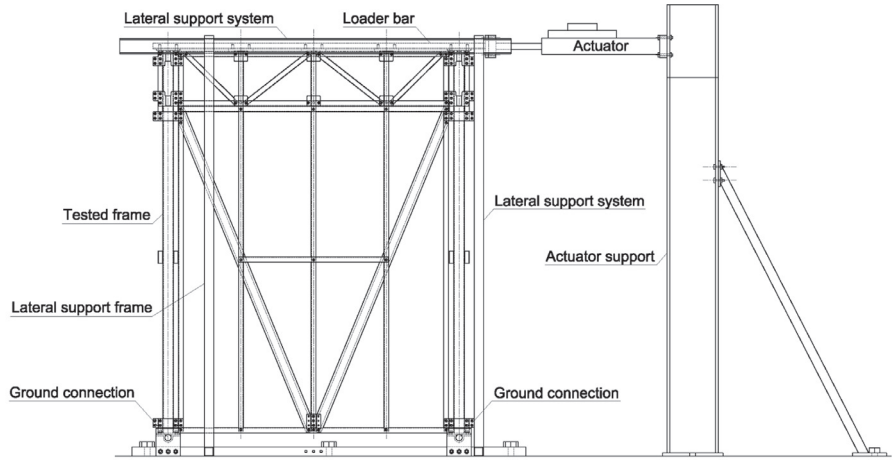

a) Load frame with V-braced panel

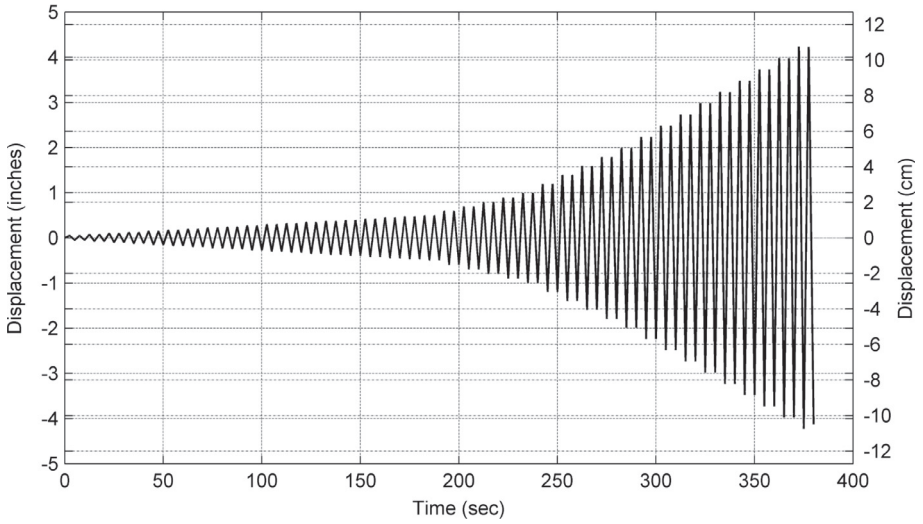

b) Test protocol for reserved-cyclic test of V-braced frame

Fig. 5. Setup for V-braced panel test.

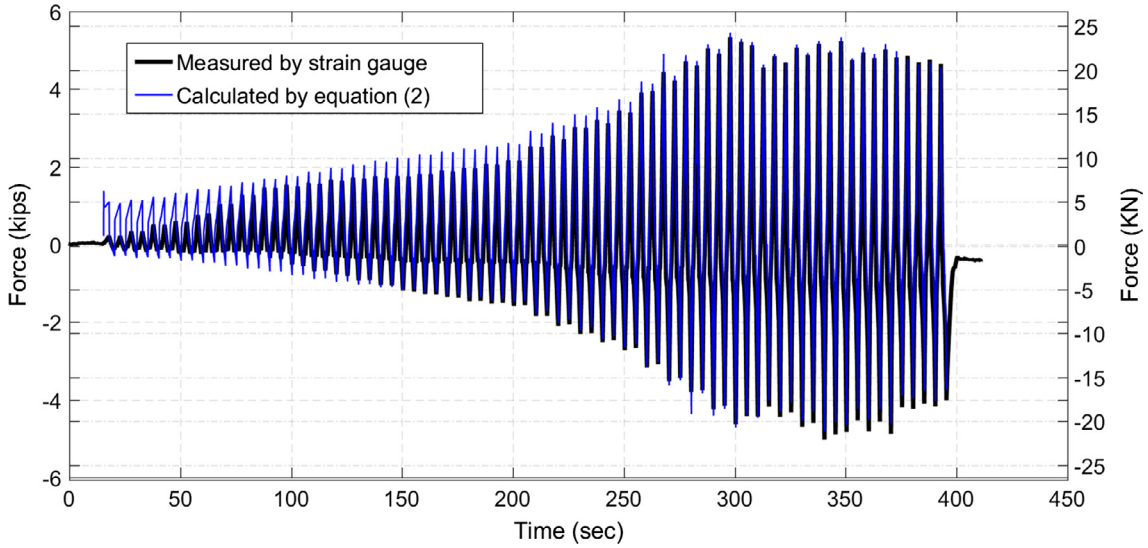

Fig. 6. The force transferred to column due to lateral displacement.

strain gauge since there was some friction in the pinned and lateral supports. After moving back and forward more than forty cycles, this friction is reduced and the force measured by the strain gauge is virtually the same as the force calculated by Eq. (2).

In the numerical model, this hysteresis is described by an eleven-parameter hysteretic model (Dao and van de Lindt [15]) which was a slight modification of the ten parameter hysteresis model introduced by Folz and Filiatrault [2]. In that hysteretic model, the envelope loading curve (hysteretic backbone) was described by five parameters: F_0, K_0, r_1, r_2, δ_u and unloading and reloading paths are described by another five parameters: F_1, r_3, r_4, α and β; the monotonic loading curve starts at the origin of the force-displacement coordinate with slope K_0 and following the envelope curve that is described by the following non-linear load-deformation relationship:

$$F = \mathrm{sgn}(\delta)(F_0 + r_1 K_0|\delta|)\left[1 - \exp\left(-\frac{K_0|\delta|}{F_0}\right)\right] \tag{24}$$

where F and δ are the force and displacement whose the relationship is described by the hysteretic model. The ultimate load is at displacement δ_u:

$$\{F_u\} = \mathrm{sgn}(\delta_u)(F_0 + r_1 K_0|\delta_u|)\left[1 - \exp\left(-\frac{K_0|\delta_u|}{F_0}\right)\right]. \tag{25}$$

At the ultimate loading point, the curve has slope r_1K_0. When the displacement goes beyond δ_u, the force starts to decrease with slope r_2K_0 to the failure point. Unloading off the envelope curve follows a path with unloading slope r_3K_0. If it continues unloading, the response moves onto a pinching path with slope r_4K_0. This pinching path always passes the pinching points $(0, F_1)$ for positive displacement increment and $(0, -F_1)$ for negative displacement increment. If it continues on the reloading then the response follows a path with degrading stiffness given by:

$$K_p = K_0\left(\frac{\delta_0}{\delta_{\max}}\right)^{\alpha} \tag{26}$$

where $\delta_0 = \frac{F_0}{K_0}$ and $\delta_{\max} = \beta\delta_{un}$, δ_{un} is the largest unloading displacement experienced by the model to that point; α and β are hysteretic parameters defining the degrading stiffness, K_p.

The ten parameters are obtained by fitting the model to the test data. In the study by Dao and van de Lindt [15], a single parameter was added to account for the degradation of the unloading slope described as parameter r_3 in the Folz and Filiatrault [2] model:

$$r_3 = r_3^{\delta u}\left(\frac{\delta_u}{\delta_{\max}}\right)^{\gamma} \tag{27}$$

where $r_3^{\delta u}$ is the unloading slope coefficient ($r_3^{\delta u}K_0$ is the unloading slope) when $\delta_{\max} = \delta_u$; γ is a parameter describing the unloading stiffness degradation. For more details on the ten-parameter hysteretic model, the interested reader is referred to Folz and Filiatrault [2]. Fig. 6d shows the V-braced panel hysteresis from the test and the best fitted model used in this example. The eleven parameters for a V-braced panel are provided in Table 1.

Recall that in Eq. (14), the equivalent lateral displacement x_{eq} calculated by Eq. (13) is used to estimate the hysteretic force using the eleven-parameter hysteretic model. In the first two load cases (static gravity and lateral loads), the hysteresis force and equivalent lateral displacement of the panel follows the backbone curve of the hysteresis. While under cyclic loading, the behavior of the panel is described by the eleven-parameter hysteretic model.

Nonlinear static analysis was conducted for the gravity and lateral load cases for both the conventional shear element model

Table 1
Eleven parameters used in fitted model.

V-braced Panel type	K_0	r_1	r_2	$r_3^{\delta u}$	r_4	F_0	F_1	δ_u	α	β	γ
2.44 m (8 ft)	9.81 KN/cm (5.6 kips/in)	0.001	−0.15	1.001	0.07	19.35 KN (4.35 kips)	1.78 KN (0.4 kips)	5.61 cm (2.21 in)	0.9	1.05	2

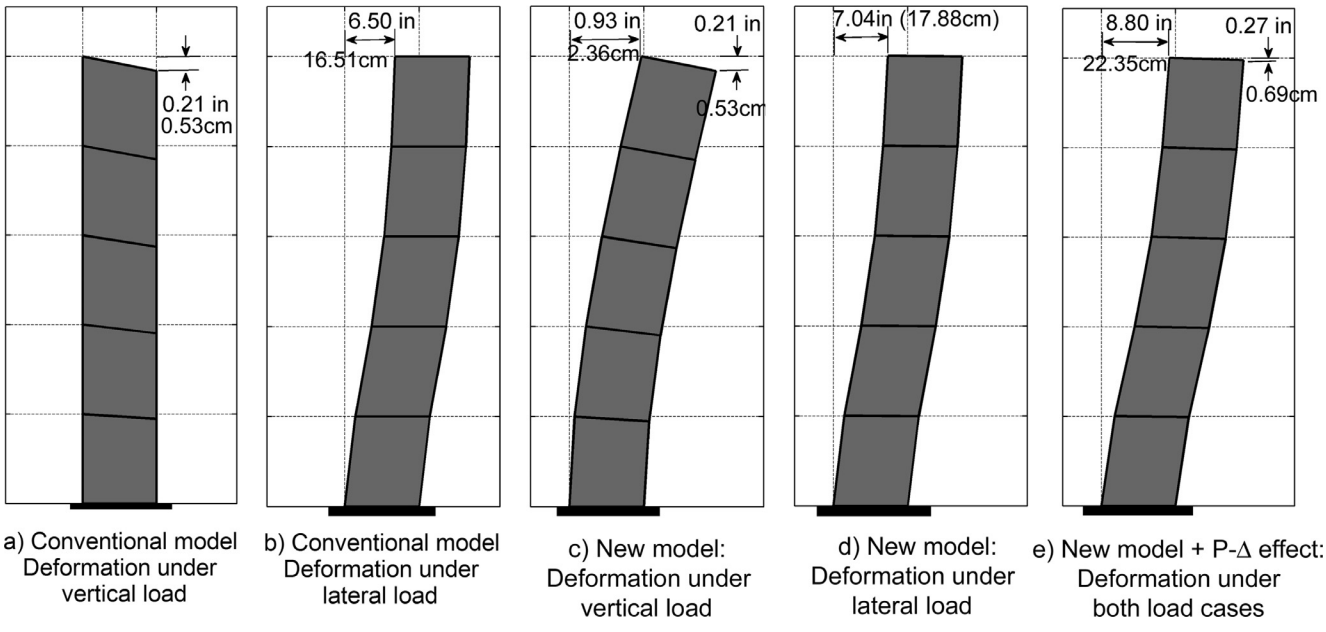

Fig. 7. Comparison of shear element deformation between conventional and new shear element models under static loads.

(SDOF) and the new shear element introduced in this study. The results from these analyses are presented in Fig. 7. In the first two analyses, the V-braced panel was modeled using a SDOF spring that considers only panel lateral drift. Because this model does not couple the lateral and vertical shear stiffness of the panel, the deformation of the frame under the first load case (asymmetric gravity load) occurs only in the vertical direction on the side that the load was applied as shown in Fig. 7a; and no lateral displacement occurs in the frame. In the second case, if the lateral load is applied on the frame, no vertical displacement occurs (Fig. 7b). In the nonlinear static analyses with the same load cases, the new shear element model was used but the P-Δ effect was not included for illustration. Fig. 7c shows the panel deformation of the frame under gravity load. As one can see from this figure, because of the coupled vertical and lateral effect, the frame does not deform only in the vertical direction on the side that the load was applied, but also experiences 2.36 cm (0.93in) displacement in the lateral direction. In the case of lateral loading (Fig. 7d), the frame has a larger lateral displacement if the new shear element model is used in the analysis (17.88 cm or 7.04in compared with 16.51 cm or 6.50in). If the deformations of the frame are compared between two models for each load case explicitly, there is not much difference (approximately 10%). But in the case where the frame is loaded in both the lateral and vertical direction, the difference in lateral deformation is approximately 23% for this example. This is exacerbated if the P-Δ effect is included, with the lateral displacement increasing by approximately 35% if the new shear element is used instead of the conventional shear element model (see Fig. 7e). This difference will increase when the vertical displacement of the columns increases as the structure becomes taller and is examined below.

In the last load case, the frame was loaded at the top with lateral reversed cyclic loading in numerical displacement control using the protocol shown in Fig. 8a. Fig. 8b shows the relationship between the lateral displacement at roof level and base shear. During the analysis, the maximum base shear of 18.42 KN (4.14 kips) was recorded. This value is approximately the same as the capacity of a single panel since the lateral resistance of the columns is typ-

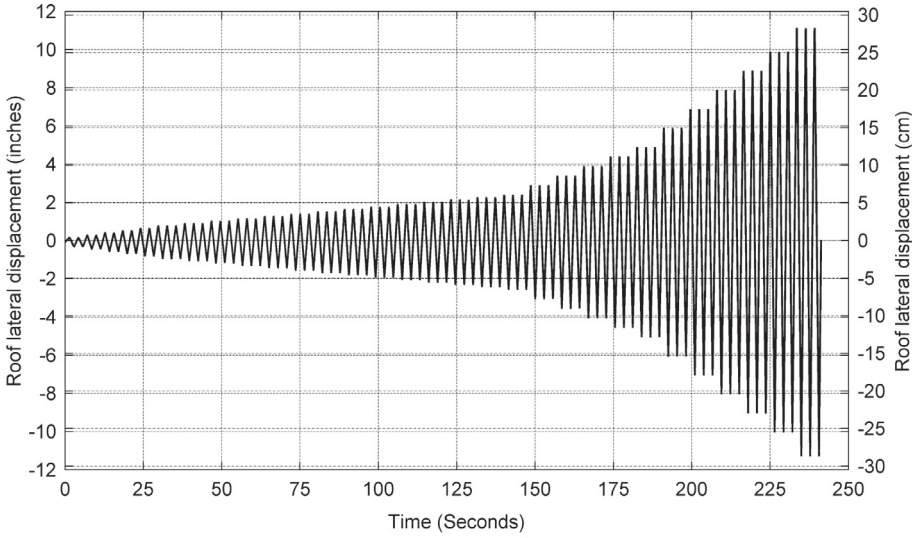

Fig. 8. Response of the frame under reversed cyclic loading.

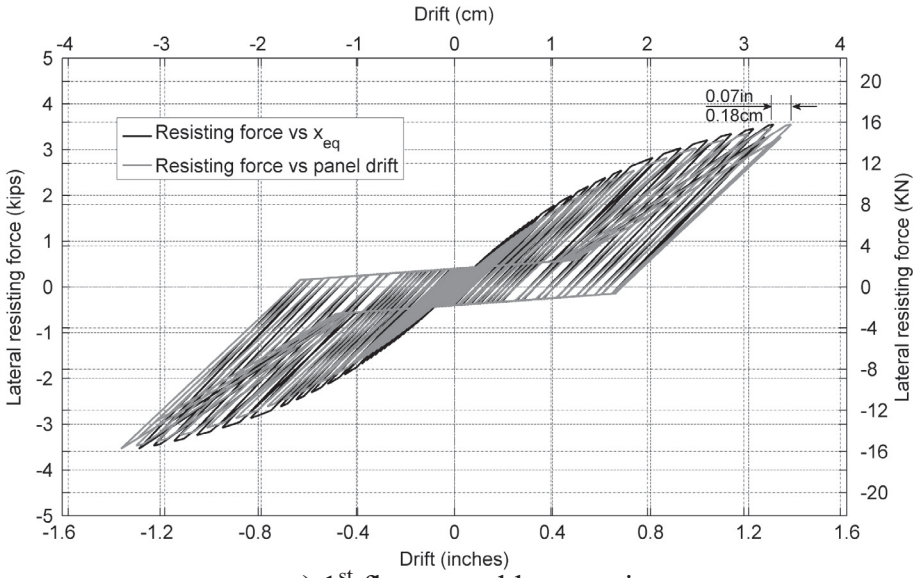

c) 1st floor panel hysteresis

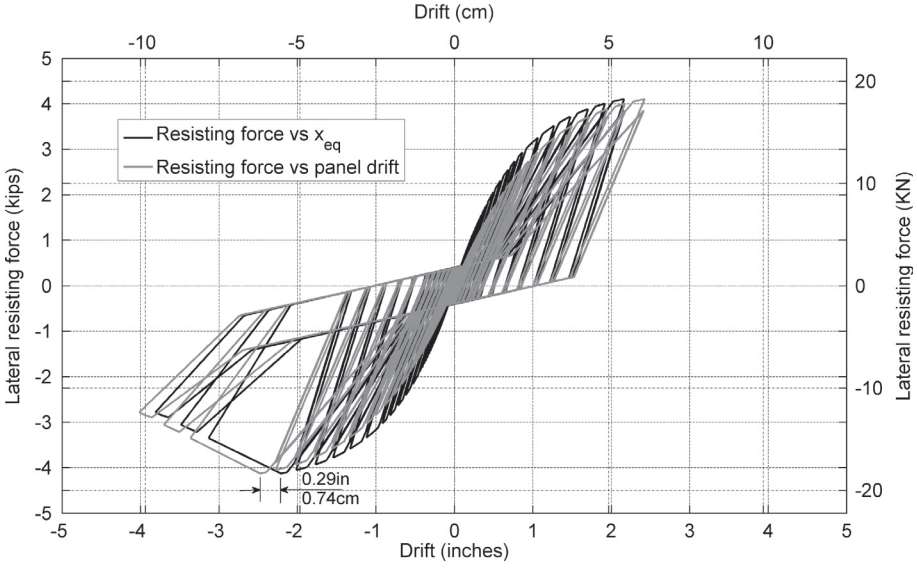

d) 5th floor panel hysteresis

Fig. 8 (*continued*)

ically insignificant. Fig. 8c shows the comparison of the hysteresis for the panels in the first floor for the same two cases described above: the plot of the panel lateral restoring force versus equivalent displacement x_{eq} and panel lateral restoring force versus panel drift. At small drifts, the lateral restoring force of the panel is small as would be expected, therefore the axial force in the column is also small (see Eq. (2)). For this reason, the axial displacement of the column and vertical displacement of the panel are both small. One can see from Fig. 8c that at the beginning, the equivalent displacement of the panel x_{eq} is about the same as the drift of the panel (Eq. (14)). When the drift in the panel increases, the difference between the panel drift and the equivalent displacement x_{eq} becomes larger as can be seen in Fig. 8c. At the maximum lateral resisting force in panel, the difference between these displacements is only 0.18 cm (0.07 in), so not a significant difference on the lowest level.

On the fifth floor, this difference is more apparent (Fig. 8d) since the vertical displacement in the panel on the fifth floor is larger than that of the panel on the first floor. In all cases, the panel drift is larger than the equivalent lateral displacement since the vertical displacement in the panels always has the opposite sign of the lateral displacement. For this reason, in order to reach the same lateral restoring force, the panels need to experience larger displacement than in the case where there is no vertical displacement. From Fig. 8c and d, one can see that the lateral resisting force in the panel on the fifth floor is larger than that of the panel on the first floor since in the first floor the columns have larger lateral resistance (the columns are assumed fixed at the base). For this reason, the panel on the fifth floor reaches the maximum lateral force before the panel on the first floor. When the panel on the fifth floor first reached the maximum lateral resisting force it softened, and the hysteresis of the frame was no longer symmetric as shown in Fig. 8b. The forces were redistributed due to the degradation of the stiffness among stories resulting in a panel hysteresis that is not symmetric as shown in Fig. 8b. This was also observed during the experiment mentioned earlier.

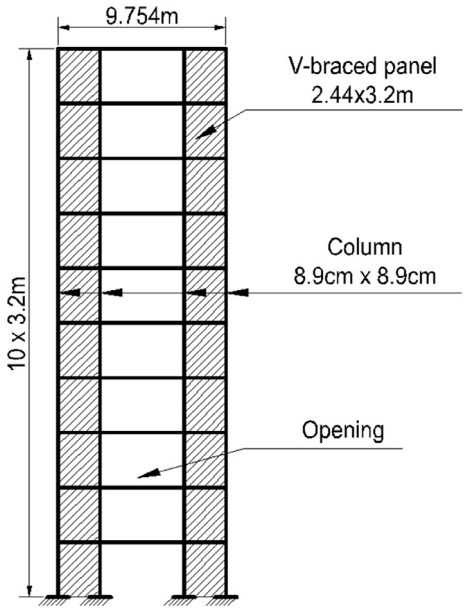

Fig. 9. Ten-story frame used in the second example.

4.2. Effects of building height

In this second example, a comparison between application of a conventional and the new shear element model is examined by analyzing frames with different heights: two stories, four stories, six stories, eight stories and ten stories. These frames have the same story configuration (panel layout, span between columns, story height) and the basic dimension of the ten-story frame shown in Fig. 9. The panels (shown by shaded area in Fig. 9) and columns used in this example have the same geometric properties as the panels and columns used in the previous example. It was assumed that these frames have loading spans of 4.9 m (16 ft) with a floor dead load of 1.15 KN/m^2 (24 psf), roof dead load of 0.81 KN/m^3 (17 psf), wall dead load of 0.44 KN/m^3 (9.1 psf) and floor live load of 1.92 KN/m^2 (40 psf) for the analysis. For each frame, the design was performed based on the equivalent lateral force procedure (ELFP) following specifications of ASCE7-10 [16]. The calculated forces for design at each floor level are shown in Table 2 for each frame.

In the ELFP, a response modification factor of $R = 6.5$ was assigned for illustrative purposes and remained consistent throughout the analysis (Table 12.2-1, ASCE7-10 [16]). During the LRFD, the resistance factor $\phi = 0.44$ was used to calculate the cold-formed steel component strength (Serrette [17]). The cross sections of the columns were kept constant for every two stories and were designed based on the load combinations specified by ASCE7-10 [16] using LRFD. For illustrative purposes, it is assumed

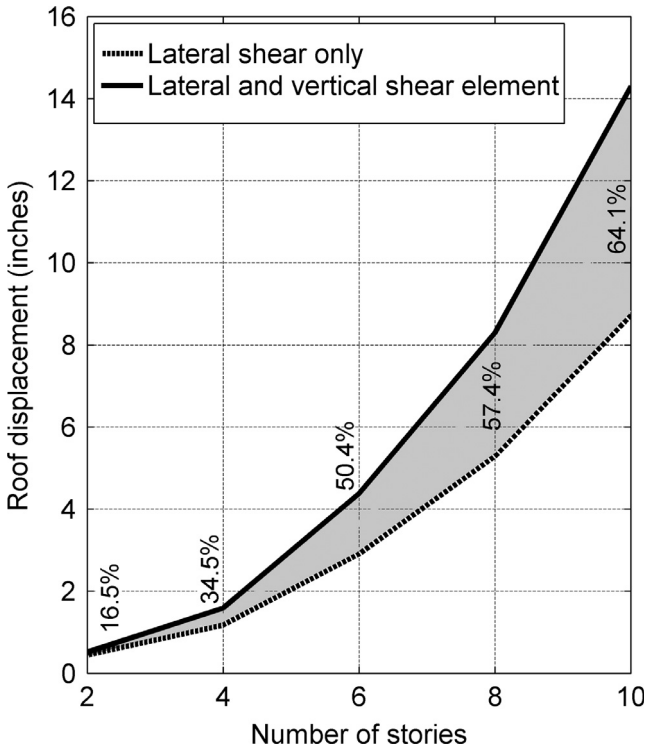

Fig. 10. Comparison between current and new models for the frame used in the last example.

that the panels and panel connections are designed so that the hysteresis of the panel is still the same as shown in Fig. 6; but the panel capacity is multiplied by a factor so that each story has the capacity that can carry the story shear calculated from the forces shown in Table 2 ($\phi = 0.44$ was used during the LRFD design procedure).

After each frame was designed, non-linear static analysis for each frame with a combination of seismic load (Table 2), dead load and live load was conducted for each frame using the conventional shear element and the new shear element model. Fig. 10 shows the comparison of the roof displacements between the two models for frames of increasing height. In Fig. 10, the dashed line shows the results from the frames in which the panels were modeled using the conventional shear element that considers only the lateral component, while the solid line represents the results for the frames in which the panels were modeled using the shear element that considers both lateral and vertical shears and displacements. The shaded area in Fig. 10 highlights the difference between the two models with the number shown in percentile providing the difference for the models. As discussed in the previous example, the vertical displacement affects the lateral displacement resulting

Table 2
Equivalent lateral force used in the second example.

Floor level	Two story frame	Four story frame	Six story frame	Eight story frame	Ten story frame
3.2 m (126in)	10.2 KN (2.3 kips)	6.2 KN (1.4 kips)	3.6 KN (0.8 kips)	1.8 KN (0.4 kips)	0.9 KN (0.2 kips)
6.4 m (252in)	12.0 KN (2.7 kips)	12.0 KN (2.7 kips)	7.1 KN (1.6 kips)	4.0 KN (0.9 kips)	2.2 KN (0.5 kips)
9.6 m (378in)	NA	18.2 KN (4.1 kips)	11.1 KN (2.5 kips)	6.7 KN (1.5 kips)	4.0 KN (0.9 kips)
12.8 m (504in)	NA	13.8 KN (3.1 kips)	15.1 KN (3.4 kips)	8.9 KN (2.0 kips)	5.8 KN (1.3 kips)
16.0 m (630in)	NA	NA	19.6 KN (4.4 kips)	11.6 KN (2.6 kips)	7.6 KN (1.7 kips)
19.2 m (756in)	NA	NA	13.8 KN (3.1 kips)	14.7 KN (3.3 kips)	9.3 KN (2.1 kips)
22.4 m (882in)	NA	NA	NA	17.3 KN (3.9 kips)	11.6 KN (2.6 kips)
25.6 m (1008in)	NA	NA	NA	11.6 KN (2.6 kips)	13.8 KN (3.1 kips)
28.8 m (1134in)	NA	NA	NA	NA	16.0 KN (3.6 kips)
32.0 m (1260in)	NA	NA	NA	NA	10.2 KN (2.3 kips)

in these significant differences between the two models. As one can see, as the building becomes taller, this effect is more and more obvious. The difference between the roof displacements for the two models is about 16.5% in a two-story building, 35.5% in a four-story building, and increases to 50.4% in a six-story building. For a ten-story building this difference is 64.1%; a result that underscores the need to consider this coupled behavior. This behavior is similar to the shear and bending displacement in a cantilever beam as the beam gets longer.

The non-linear static analysis was implemented for above examples, under the cyclic displacement – controlled loading. Based on the experimental test for a V-braced panel, the hysteretic behavior of the panel was obtained and used to calibrate the Folz and Filiatrault [2] hysteretic model. This model was applied to calculate the lateral stiffness k_{xx} of the shear wall element. After each step, the value of k_{xx} was updated. Therefore, this model is capable of utilizing for nonlinear dynamic analysis. The dynamic analysis procedure can refer to Folz and Filiatrault's study [18,19], in which a simple and versatile numerical model was introduced to predict the dynamic characteristics, quasi-static pushover and seismic response of light-frame wood buildings.

5. Summary and conclusions

In this study, a new shear element for use in nonlinear finite element modeling is introduced. This new shear element couples the lateral and vertical stiffness of a shear wall structure. It can be used to describe the shear behavior of shear walls for light-frame structures. For nonlinear analysis, the nonlinear behavior of the shear wall structure can be described through the lateral stiffness k_{xx} of the shear element stiffness matrix. With that consideration, no condensation technique is needed to reduce the number of nodes for the substructure model. The application of the shear element was explained through examples presented in this paper. The behavior of the shear element was examined for both lateral and vertical loads. The analysis results showed that with the effect of vertical displacement of the shear element included, the lateral displacement on the top of a frame increases with height and becomes significant for mid-rise (4–6 story) heights. If this effect is considered in combination with the P-Δ effect, the increase in lateral displacement may be as high as to 64.1% for the ten-story frame shown in the second example. The analysis in this study also shows that the new shear element is capable of modeling the behavior of shear panels in mid-rise or tall buildings. This new shear element can be used in the nonlinear analysis for both static and dynamic loading.

However, the proposed shear wall element was just verified by comparing measured vertical forces transferred from the wall to columns and the calculated forces from model. A comparison between the proposed model and detailed finite element models might be needed. The relationship between the lateral and vertical stiffness, the effects the width and the height of the shear wall on the combined stiffness should be consider in further studies.

Acknowledgement

The cold-formed steel panel used in the example is part of The Uniform Truss Construction System (UTCS). The UTCS is a product of The Prescient Companies, LLC and patents are pending on the system. The information, specimens, and funding for this study was provided by The Prescient Companies, LLC, and that support is gratefully acknowledged. Detailed assistance was provided by Michael Lastowski and John Vanker of TPC.

References

[1] Collins M, Kasal B, Paevere P, Foliente GC. Three-dimensional model of light frame wood buildings. I: Model description. ASCE. J Struct Eng 2005;131(4):676–83.
[2] Folz B, Filiatrault A. Cyclic analysis of wood shear walls. ASCE J Struct Eng 2001;127(4):433–41.
[3] Pang W, Rosowsky DV, Pei S, van de Lindt JW. Evolutionary parameter hysteretic model for wood shear walls. ASCE J Struct Eng 2007;133(8):1118–29.
[4] Pei S, van de Lindt JW. Coupled shear-bending formulation for seismic analysis of stacked wood shear wall systems. Earthquake Eng Struct Dynam 2009;38(6):1631–47.
[5] Xu J, Dolan JD. Development of a wood-frame shear wall model in ABAQUS. ASCE J Struct Eng 2009;135(8):977–84.
[6] Kim TW, Wilcoski J, Foutch DA, Lee MS. Shaketable tests of a cold-formed steel shear panel. Eng Struct 2006;28(10):1462–70.
[7] Pastor N, Rodríguez-Ferran A. Hysteretic modeling of X-braced shear walls. Thin-Walled Struct 2005;43(10):1567–88.
[8] Fulop LA, Dubina D. Performance of wall-stud cold-formed shear panels under monotonic and cyclic loading. Part II: Numerical modelling and performance analysis. Thin-Walled Struct 2004;42:339–49.
[9] Shamim I, Rogers CA. Steel sheathed/CFS framed shear walls under dynamic loading: numerical modelling and calibration. Thin-Wall Struct 2013;71:57–71.
[10] Leng J, Schafer BW, Buonopane SG. Modeling the seismic response of cold-formed steel framed buildings: model development for the CFS-NEES building. Proceedings of the annual stability conference – Structural stability research council, St. Louis, Missouri, April 16–20, 2013.
[11] Martínez-Martínez J, Xu L. Simplified nonlinear finite element analysis of buildings with CFS shear wall panels. J Constr Steel Res 2011;67:565–75.
[12] Petersson H, Popov EP. Substructuring and equation system solutions in finite element analysis. Comput Struct 1977;1977(7):197–206.
[13] Lee DG, Kim HS, Chun MH. Efficient seismic analysis of high-rise building structures with the effects of floor slabs. Eng Struct 2002;24(5):613–23.
[14] Kim HS, Lee DG. Analysis of shear wall with openings using super elements. Eng Struct 2003;25(3):981–91.
[15] Dao TN, van de Lindt JW. Seismic performance of an innovative light-frame cold-formed steel frame for mid-rise construction. ASCE J Struct Eng 2013;139(5):837–48.
[16] American Society of Civil Engineers. Minimum design loads for buildings and other structures, ASCE/SEI 7-10. Reston, VA: ASCE; 2010.
[17] Serrette R. Seismic design strength of cold-formed steel-framed shear walls. ASCE J Struct Eng 2010;136(9):1123–30.
[18] Folz B, Filiatrault A. Seismic analysis of woodframe structures. I: Model formulation. ASCE. J Struct Eng 2004;130(9):1353–60.
[19] Folz B, Filiatrault A. Seismic analysis of woodframe structures. II: Model implementation and verification. ASCE. J Struct Eng 2004;130(9):1361–70.